Zero : Jurnal Sains, Matematika, dan Terapan
E-ISSN : 2580-5754; P-ISSN : 2580-569X
Volume 10, Number 2, 2026
DOI: 10.30829/zero.v10i2.31716
Page: 881-895



Fractal Dimension and K-Nearest Neighbor Analysis for Turtle Species Classification Based on Carapace Pattern Complexity

[1]Nadya Nafis Kartosen
Department of Mathematics, Universitas Negeri Surabaya, Surabaya, 60231, Indonesia

[2]Dwi Juniati
Department of Mathematics, Universitas Negeri Surabaya, Surabaya, 60231, Indonesia

Article Info

Article history:

Accepted: 10 October 2026

Keywords:

Box-Counting;
Carapace Pattern;
Fractal Dimension;
K-Nearest Neighbor;
Species Classification.

ABSTRACT

Accurate turtle species identification supports biodiversity monitoring and conservation. This study classified seven turtle species using box-counting fractal dimension a single scalar numerical feature and K-Nearest Neighbor (K-NN) based on carapace pattern complexity. A dataset of 140 dorsal carapace images (20 per species) was compiled from iNaturalist Research Grade observations via random sampling with rejection-based screening against predefined inclusion criteria. Images were preprocessed (crop, resize, Gaussian smoothing, grayscale, Otsu thresholding, Canny edge detection) prior to fractal-dimension extraction. Stratified 3-, 5-, 7-, and 10-fold cross-validation was repeated over ten fixed random seeds. The best-performing observed configuration (10-fold, K = 3) achieved 87.14% ± 0.48% accuracy and 86.75% pooled macro-F1. A dataset-matched GLCM baseline achieved 61.14% ± 1.76% accuracy under the same setting, with a highly significant paired difference (paired t-test, $p < 0.001$; Wilcoxon signed-rank, $p = 0.001953$).

This is an open access article under the CC BY-SA license.

Corresponding Author:

Dwi Juniati,
Department of Mathematics
Universitas Negeri Surabaya, Indonesia
Email: dwi_juniati@unesa.ac.id

1. INTRODUCTION

Turtles, classified in the order Testudines, are among the oldest surviving groups of reptiles and are characterized by a hard shell consisting of a dorsal carapace and a ventral plastron. Despite their long evolutionary history and resilience, turtles and tortoises remain among the most threatened groups of vertebrates worldwide. Recent global assessments indicate that extinction risk among chelonians is associated with large body size, restricted geographic ranges, and intense anthropogenic pressures, with the Indomalayan region identified as a major hotspot for threatened biodiversity [1]. A comprehensive global assessment of reptiles also reported significant extinction risks for various reptile species and emphasized the need for targeted conservation efforts for turtles and crocodilians [2]. These conditions underscore the importance of reliable species identification for biodiversity monitoring and conservation.

These conservation challenges are further exacerbated by wildlife trade. Several turtle species listed under CITES continue to be collected and traded in Indonesia, while market-based studies have reported difficulties in distinguishing legal trade from illegal harvesting, as well as violations or circumvention of quota and permitting regulations [3]. Recent economic research also indicates that legally permitted trade in freshwater turtles provides limited and geographically uneven livelihood benefits to collectors, raising concerns about the sustainability of

current harvesting practices [4]. In response to these challenges, artificial intelligence (AI) and image-based technologies have increasingly been explored for wildlife identification and trade enforcement, including AI-assisted photographic identification for CITES enforcement [5] and machine learning approaches to distinguish acoustically similar wildlife species involved in trade [6]. These developments highlight the need for accurate and objective species identification approaches to support conservation monitoring and enforcement.

Turtle species identification has traditionally relied on expert assessment of morphological characteristics, particularly carapace and plastron features such as shell shape, dome height, and scute coloration [7]. Although these characteristics provide important taxonomic information, manual identification requires specialized expertise and can be time-consuming and subjective. Consequently, image-based computational methods have increasingly been investigated as alternatives for automated species identification [8]. Deep learning approaches have demonstrated the feasibility of image-based turtle classification, including the classification of turtles imported into Korea and ensemble-based classification of turtle species [9], [10]. Multiview deep-learning methods have also been applied to fine-grained classification of closely related *Malayemys* species [8]. Beyond turtles, computational image analysis has been widely used for wildlife recognition and identification, including ecological camera-trap imagery, lightweight machine-learning systems, dorsal carapace imagery for individual sea-turtle recognition, and morphological measurements combined with machine-learning classifiers for cryptic species discrimination [11], [12], [13], [14]. While these studies demonstrate the potential of computational approaches, they predominantly rely on deep-learning architectures or conventional morphological, color, and texture representations. The geometric complexity of turtle carapace patterns remains comparatively unexplored as a compact quantitative feature.

Fractal dimension offers a mathematical representation of the geometric complexity of irregular structures and can be estimated from digital images using box-counting methods. Previous studies have examined methodological aspects of box-counting estimation [15], its limitations for complex biological boundaries [16], and its application to species discrimination and biometric recognition [17], [18]. Fractal dimension has also been used as an input feature for classification methods, including K-Nearest Neighbor (K-NN) and other machine-learning approaches [19], [20], [21]. Similarly, texture descriptors such as Gray-Level Co-occurrence Matrix (GLCM) features have been combined with K-NN for image classification tasks [22], [23]. These studies establish the potential of fractal and texture-based representations for classification but do not directly address turtle carapace pattern complexity. In the present study, fractal dimension is deliberately evaluated as a single scalar feature, rather than using a multifractal spectrum, lacunarity, or a combination of multiple texture descriptors. This choice provides a compact and computationally efficient representation that allows the classification capability of geometric pattern complexity itself to be evaluated directly, while avoiding the additional dimensionality and interpretive complexity introduced by multi-feature representations. K-NN is consequently appropriate for this setting because it can classify low-dimensional numerical representations based on feature similarity [24]. Because fractal dimension is estimated after image preprocessing, the influence of image resolution, Gaussian smoothing, and edge-detection thresholds is also examined through sensitivity analysis to assess the robustness of the resulting feature.

However, existing turtle-identification studies have focused primarily on deep-learning-based image classification [8], [9] or conventional morphological, color, and texture features, leaving the geometric complexity of carapace patterns insufficiently investigated as a quantitative representation. Moreover, previous applications of box-counting fractal dimension have largely concerned non-shell biological structures and other image domains [16], [19], which differ substantially from carapace patterns in terms of structural regularity and complexity. The combination of box-counting fractal dimension with K-NN classification for turtle carapace patterns has therefore received limited attention, particularly in the Indonesian context. Box-counting fractal dimension was selected because it provides a quantitative and computationally efficient measure of the complexity of irregular carapace patterns [15], [16]. However, because the feature is calculated after preprocessing, its reliability may be affected by segmentation quality, image resolution, illumination conditions, and camera angle. K-NN is suitable for classification using low-dimensional numerical features, making it appropriate for evaluating fractal dimension values as classification inputs.

Building on this research gap, the present study classifies seven turtle species *Trachemys scripta elegans, Manouria emys, Centrochelys sulcata, Geochelone elegans, Stigmochelys pardalis, Testudo hermanni,* and *Heosemys spinosa* representing a range of IUCN conservation statuses [25], [26] based on carapace pattern complexity using box-counting fractal dimension and K-NN. Classification performance was evaluated using four-fold-count schemes, namely 3-fold, 5-fold, 7-fold, and 10-fold stratified cross-validation, with K values of 3, 5, 7, and 9. The cross-validation procedure was repeated using ten fixed random seeds (1-10) to assess the stability of the results. In addition, sensitivity analysis was performed to examine the effects of image resizing, Gaussian filtering, and Canny threshold settings on fractal-dimension estimation. Therefore, this study aimed to evaluate whether a single box-counting fractal-dimension value can represent turtle carapace pattern complexity sufficiently for species classification and to identify the best-performing observed K-NN configuration among the evaluated experimental settings.

2. RESEARCH METHOD

2.1 Research Design and Data

This study employed a quantitative computational approach to classify seven turtle species based on carapace pattern complexity. Fractal-dimension values extracted using the box-counting method served as numerical features, while species identity served as the classification target.

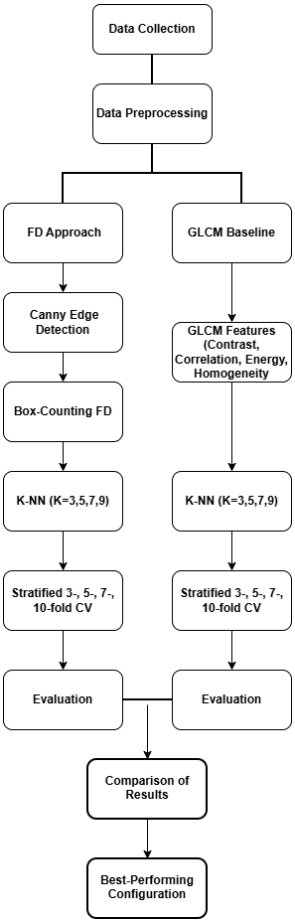


Figure 1. Research Procedure Flowchart

The secondary data used in this study consisted of dorsal carapace images obtained from the citizen-science platform iNaturalist (https://www.inaturalist.org) in JPG format. A total of 140 images were collected, comprising 20 images from each of seven turtle species. This sample size and its implications for statistical power and generalizability are discussed in Section 3.7. The seven species represented a range of IUCN conservation statuses, from Critically Endangered to Least Concern, as summarized in Table 1 [25], [26].

Table 1. Characteristics of the Seven Turtle Species Used in This Study

Species	Family	Carapace Characteristics	IUCN Status
Trachemys scripta elegans	Emydidae	Oval, light brown with yellow stripes, serrated marginal scutes	Least Concern
Manouria emys	Testudinidae	Flattened, concentric growth ring pattern, serrated anterior-posterior margins	Critically Endangered
Centrochelys sulcata	Testudinidae	Dome-shaped, yellowish brown with dark brown scute borders	Endangered
Geochelone elegans	Testudinidae	Star-shaped radiating yellow lines on a dark background	Vulnerable
Stigmochelys pardalis	Testudinidae	High-domed, irregular black blotches on a cream to yellowish background	Least Concern
Testudo hermanni	Testudinidae	Domed, yellow to olive green with dark brown to black blotches	Near Threatened
Heosemys spinosa	Geoemydidae	Oval, brown to blackish brown with sharply serrated marginal scutes	Endangered

For each species, 20 images were randomly selected from iNaturalist Research Grade observations and screened according to three inclusion criteria: (1) a clear dorsal view of the carapace, (2) minimal obstruction by other body parts or background objects, and (3) sufficient image resolution to allow the carapace pattern to be observed. Representative dorsal carapace images of the seven turtle species included in the dataset are shown in Figure 2.



(a) Trachemys scripta elegans *(b) Manouria emys* *(c) Centrochelys sulcata* *(d) Geochelone elegans*



(e) Stigmochelys pardalis *(f) Testudo hermanni* *(g) Heosemys spinosa*

Figure 2. Images of the Seven Turtle Species
(Source: iNaturalist observations, accessed in 2026)

2.2 Image Preprocessing and Fractal Dimension

Each image was manually cropped to isolate the carapace region, excluding the head, limbs, and extraneous background, and then resized to 200 × 100 pixels. The resized RGB image was converted to grayscale using the luminance transformation:

$$Grayscale = (R \times 0.2989) + (G \times 0.5870) + (B \times 0.1140) \quad (1)$$

where R, G, and B denote the red, green, and blue intensity components, respectively. A Gaussian filter with $\sigma = 2$ was then applied to the grayscale image to reduce image noise. The grayscale image was subsequently segmented using Otsu's automatic thresholding method [27]. The binary image was expressed as:

$$s(x,y) = \begin{cases} 1, \text{if } f(x,y) \geq T \\ 0, \text{if } f(x,y) < T \end{cases} \quad (2)$$

To separate the foreground carapace-pattern structures from the background and produce a binary representation. Canny edge detection was then applied to the resulting binary image [28] . In this workflow, the binary image served as an intermediate representation that constrained the edge-detection step to the segmented foreground structure, while Canny was used to identify the boundaries within that representation. Consequently, the box-counting procedure quantified the geometric complexity of the edges derived from the Otsu segmented image rather than intensity gradients from the original grayscale image. Fractal dimension values were calculated from each edge-detected image using the box-counting method, based on fractal geometry theory [29], with methodological considerations regarding grid-size selection and box-counting estimation [15] and the practical scope and limitations of box-counting fractal analysis for complex biological boundary structures [16]. In this method, the edge image was covered with square boxes of different sizes, and the number of boxes containing at least one edge pixel was counted. The relationship between the number of occupied boxes $N(r)$ and the box size r is expressed as:

$$N(r) = \frac{1}{r^D} \quad (3)$$

where $N(r)$ denotes the number of occupied boxes, r is the box size, and D is the fractal dimension. Taking the logarithm gives:

$$log(N(r)) = D\, log\left(\frac{1}{r}\right) \quad (4)$$

$$D = \frac{log\, N(r)}{log\left(\frac{1}{r}\right)} \quad (5)$$

The fractal dimension D was then obtained as the slope (α) of the linear regression between $\log(N(r))$ and $\log\left(\frac{1}{r}\right)$, calculated as:

$$\alpha = \frac{n(\sum_k^n xy) - (\sum_{k=1}^n x)(\sum_{k=1}^n y)}{n(\sum_{k=1}^n x^2) - (\sum_{k=1}^n x)^2} \quad (6)$$

where $x = \log\left(\frac{1}{r}\right)$, $y = \log(N(r))$, and $n$denotes the number of box-size scales used in the regression . The resulting fractal dimension quantified the geometric complexity of each carapace pattern and was used as the numerical feature for the subsequent K-NN classification.

The box-counting procedure was implemented as a custom MATLAB function rather than a built-in routine. Each 200 × 100-pixel edge image was zero-padded to a square image of size $2^p \times 2^p$, where (p) was the smallest integer satisfying $2^p \geq 200$. Thus, $(p = 8)$, resulting in a 256×256 pixels padded image. Box sizes were defined as powers of two, $(r = 2^0, 2^1 \ldots, 2^{(p-1)})$ pixels, corresponding to (1, 2, 4, 8, 16, 32, 64, and 128) pixels, giving $(n = 8)$ scales. The largest box size, $(r = 2^8 = 256)$ pixels was excluded from the regression because it produces a single trivial count covering the entire image. For each box size, (N(r)) was obtained by counting the number of non-overlapping $r \times r$ blocks containing at least one edge pixel. The fractal dimension was then estimated using an ordinary least-squares linear regression (polyfit in MATLAB) fitted to the eight pairs of $\log(N(r))$, against $\log\left(\frac{1}{r}\right)$.

2.3 Sensitivity Analysis

A sensitivity analysis was conducted to examine the effect of selected image-processing parameters on the extracted fractal dimension. Three preprocessing factors were evaluated: image resolution, Gaussian-filter parameter, and Canny edge-detection threshold. For image resolution, three sizes were compared: $150 \times 75, 200 \times 100, and\ 250 \times 125$ pixels. For Gaussian filtering, $\sigma = 1$, $\sigma = 2$, $and\ \sigma = 3$ were evaluated. The Canny edge detector was evaluated using the automatic threshold and three manually specified threshold ranges: $[0.05, 0.15]$, $[0.10, 0.20]$, $and\ [0.15, 0.30]$. The relative difference between an alternative configuration and the reference configuration was calculated as:

$$RD = \frac{|D_{alt} - D_{ref}|}{D_{ref}} \times 100\% \quad (7)$$

Where D_{alt} denotes the mean fractal dimension obtained using the alternative configuration and D_{ref} denotes the mean fractal dimension obtained using the reference configuration of 200 × 100 pixels, $\sigma = 2$, and automatic Canny thresholding. Crop tightness and Otsu thresholding were not independently varied because the cropping procedure was standardized and Otsu thresholding was adaptively determined for each image. Otsu's method determines an automatic global threshold based on the gray-level histogram [27]. The sensitivity results were used to assess the extent to which the estimated fractal dimension changed under alternative preprocessing configurations.

2.4 K-NN Classification and Cross-Validation

The resulting fractal-dimension values were classified using the K-Nearest Neighbor (K-NN) algorithm. Because each image was represented by a single fractal-dimension value, the main experiment constituted a one-dimensional feature space. Accordingly, the Euclidean distance between a training sample x and a validation sample y reduced to the absolute difference between their fractal-dimension values:

$$D(x, y) = |x - y| \quad (8)$$

where $D(x, y)$ represents the distance between the fractal-dimension value x of a training sample and the fractal-dimension value y of a validation sample. Classification followed the standard K-NN procedure [24]. For each validation sample, the distance to all training samples was calculated using Equation (8), the resulting distances were sorted in ascending order, the K nearest training samples were selected as neighbors, and the predicted class was determined based on the majority class among the selected neighbors.

Model performance was evaluated using stratified k-fold cross-validation with four-fold-count schemes: 3-fold, 5-fold, 7-fold, and 10-fold. Stratified k-fold cross-validation was adopted because it maintains approximately equal class proportions across folds and improves the stability of accuracy estimates relative to non-stratified sampling, particularly for datasets with a limited number of samples per class [30]. The dataset was partitioned into k subsets of approximately equal size, $D_1, D_2, \ldots, D_k$. In each of

the $k$iterations, one subset $D_i$served as the validation set while the remaining $k-1$ subsets served as the training set. This procedure was repeated until every subset had been used as the validation set exactly once.

To prevent data leakage, fractal dimension was extracted independently for each image prior to cross-validation, since this image level operation like the preceding grayscale conversion, Gaussian filtering, and Otsu thresholding used neither class labels nor information derived from other images. Within each fold, the mean and standard deviation used for feature normalization were computed exclusively from the training subset and then applied to both the training and validation subsets, ensuring that validation data never contributed to the estimation of normalization parameters. This procedure reduced the risk of data leakage and provided a more appropriate estimate of model performance under the evaluated cross-validation schemes [31]. Classification performance was evaluated using four neighborhood sizes, K = 3, 5, 7, and 9, to examine the effect of neighborhood size on classification accuracy.

For the dataset matched baseline, Gray-Level Co-occurrence Matrix (GLCM) texture features were extracted from the same 140 preprocessed images after grayscale conversion, without the Otsu and Canny stages used for fractal-dimension extraction. The grayscale images were quantized to 32 gray levels. GLCMs were computed using distances of 1, 2, and 4 pixels and directions of $0°, 45°, 90°,$ and $135°$, with symmetric matrices. Four texture descriptors contrast, correlation, energy, and homogeneity were calculated and averaged across all selected distances and directions. These features were classified using the same K-NN values, stratified fold-count schemes, ten fixed random seeds, and training-fold-only normalization as the fractal-dimension experiment.

2.5 Evaluation Metrics and Software

Classification accuracy was calculated as:

$$Accuracy = \sum_{c=1}^{C} \frac{TP_c}{N} \times 100\% \tag{9}$$

where TP_c denotes the number of correctly classified samples belonging to class c, $C$is the number of classes, and N is the total number of evaluated samples. For multiclass evaluation, precision and recall for each species were calculated as:

$$\text{Precision} = \frac{TP}{TP + FP} \tag{10}$$

and

$$\text{Recall} = \frac{TP}{TP + FN} \tag{11}$$

The F1-score for each species was calculated using:

$$\text{F1} = 2\frac{Precision \times Recall}{Precision + Recall} \tag{12}$$

For statistical comparison among K-NN configurations, paired Wilcoxon signed-rank tests were applied to the ten seed-level accuracies of the 10-fold experiments, comparing K = 3 with K = 5, K = 7, and K = 9. Holm correction was applied to the three pairwise comparisons, with a significance level of $\alpha = 0.05$. For the dataset-matched comparison between fractal dimension and GLCM, paired t-test and Wilcoxon signed-rank test were applied to the ten corresponding seed-level accuracies under the same 10-fold, K = 3 setting. Macro-F1 was calculated as the arithmetic mean of the F1-scores across the seven species, where $C = 7$ represents the number of species:

$$\text{Macro} - \text{F1} = \frac{1}{C}\sum_{c=1}^{C} F1_c \tag{13}$$

All computational procedures were implemented using MATLAB R2026a. This study did not involve direct handling, capture, or manipulation of live animals. All images were secondary data obtained from a publicly accessible citizen-science database.

3. RESULT AND ANALYSIS

3.1 Image Processing

Image processing was performed using MATLAB to convert the original dorsal carapace photographs into edge representations suitable for fractal-dimension analysis. The images were first cropped to retain the carapace region, resized to 200 × 100 pixels, converted to grayscale, and smoothed using a Gaussian filter with $\sigma = 2$. The grayscale images were then segmented using Otsu's thresholding method and processed using Canny edge detection to extract the scute boundary patterns used for fractal-dimension calculation. The resulting edge images represented the structural boundaries of the carapace patterns. These edge structures were subsequently used as input for the box-counting procedure.

Table 2. Example of Image Processing Results for Each Turtle Species

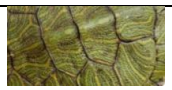
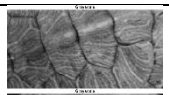
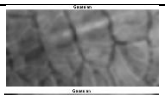
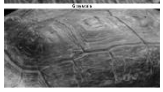
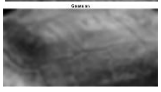
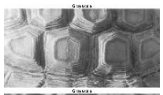
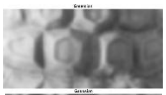
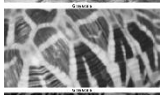
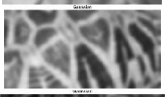
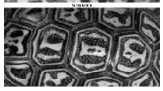
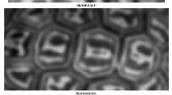
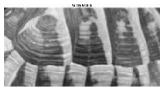
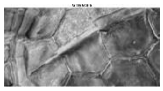
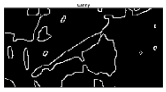
Turtle Species	Original Image	Grayscale Image	Gaussian Filter	Binary Image	Canny Edge Detection Result
Trachemys scripta elegans					
Manouria emys					
Centrochelys sulcata					
Geochelone elegans					
Stigmochelys pardalis					
Testudo hermanni					
Heosemys spinosa					

Table 2 shows the results of the image-processing stages applied to representative carapace images from the seven turtle species. The preprocessing procedure transformed the original images into binary and edge representations, with the final Canny edge images emphasizing the structural boundaries of the carapace patterns used for fractal-dimension estimation.

3.2 Box-Counting Fractal Dimension

Fractal dimension values were calculated for each processed carapace image using the box-counting method implemented in MATLAB. Across the entire dataset, the resulting values ranged from 0.9337 to 1.5375, indicating variation in the complexity of the extracted carapace patterns among the seven turtle species. The distribution of fractal-dimension for the seven species is presented in Figure 3.

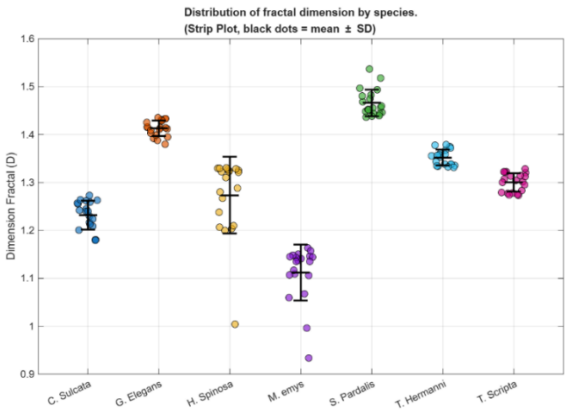


Figure 3. Distribution of fractal dimension by species

The distribution shows relatively distinct concentrations of fractal-dimension values among several species, although some overlap remains. *Manouria emys* generally occupied the lower fractal-dimension range, whereas *Stigmochelys pardalis* occupied the higher range. *Heosemys spinosa* showed comparatively greater within-species variability, as indicated by its relatively large standard deviation and broad range of fractal-dimension values.

Table 3. Fractal Dimension Statistics for Each Turtle Species

Species	n	Mean ± SD	Minimum	Maximum
Trachemys scripta elegans	20	1.3002 ± 0.0192	1.2736	1.3287
Manouria emys	20	1.1122 ± 0.0583	0.9337	1.1637
Centrochelys sulcata	20	1.2317 ± 0.0300	1.1800	1.2729
Geochelone elegans	20	1.4134 ± 0.0164	1.3801	1.4350
Stigmochelys pardalis	20	1.4662 ± 0.0280	1.4361	1.5375
Testudo hermanni	20	1.3522 ± 0.0164	1.3320	1.3787
Heosemys spinosa	20	1.2734 ± 0.0801	1.0047	1.3305

Among the seven species, *Manouria emys* exhibited the lowest mean fractal dimension (1.1122 ± 0.0583), whereas *Stigmochelys pardalis* exhibited the highest mean (1.4662 ± 0.0280). *Manouria emys* also had the lowest observed value (0.9337), while *Stigmochelys pardalis* had the highest observed value (1.5375). In contrast, *Heosemys spinosa* showed the largest standard deviation (0.0801) and the widest fractal-dimension range (1.0047–1.3305), indicating greater within-species variability. Its distribution overlapped with several other species, particularly *Trachemys scripta elegans* and *Centrochelys sulcata*. Such overlap may contribute to misclassification when only fractal dimension is used as the input feature. Overall, the results indicate that fractal dimension captured differences in the structural complexity of the extracted carapace patterns. However, the overlapping ranges also indicate that this single scalar feature did not completely separate all seven species.

A one-way ANOVA was conducted to further evaluate whether the mean fractal dimension differed among the seven turtle species. Because within-species standard deviations varied considerably (e.g., 0.0801 for Heosemys spinosa versus 0.0280 for Stigmochelys pardalis), Levene's test was first used to check the homogeneity of variance assumption; it indicated significant heterogeneity of variance across species (Brown–Forsythe $W = 3.17$, $p = 0.0062$), so a Welch ANOVA, which does not assume equal variances, was used in place of the standard one-way ANOVA. The Welch ANOVA produced a statistically significant result, $F(6, 58.18) = 226.67$, $p = 1.95 \times 10^{-38}$, confirming that the conclusion of significant differences in mean fractal dimension among species is robust to the unequal variance violation. For reference, the standard (equal-variance) one-way ANOVA gave a similarly significant but not directly comparable result, $F(6, 133) = 157.17$, $p = 7.45 \times 10^{-58}$ (not corrected for unequal variances). Together, these results provide statistical support that fractal dimension captured systematic differences in carapace pattern complexity across the studied species; given the astronomically small p-values from both tests, this difference should be interpreted as strong evidence of unequal group means rather than over-interpreted in terms of its exact magnitude. However, the significant overall difference does not indicate complete class separation, as overlapping fractal-dimension ranges were still observed among several species.

3.3 Sensitivity Analysis

The sensitivity analysis showed that the extracted fractal dimension was more affected by image resolution and Gaussian smoothing than by the tested Canny threshold settings.

Table 4. Relative Changes in Fractal Dimension under Different Preprocessing Parameters

Species	Resize Change	Gaussian Change	Canny Change
Trachemys scripta elegans	6.66–7.25%	6.51–8.81%	0.03–0.16%
Manouria emys	6.18–8.25%	4.60–9.89%	0.01–0.10%
Centrochelys sulcata	4.79–6.52%	4.82–8.11%	0.10–0.26%
Geochelone elegans	4.01–5.01%	3.28–3.38%	0.06–0.13%

Stigmochelys pardalis	5.91–6.08%	5.14–5.81%	0.19–0.23%
Testudo hermanni	4.07–5.38%	3.45–4.20%	0.01–0.06%
Heosemys spinosa	5.15–6.17%	3.69–6.37%	0.02–0.03%

Departing from the reference configuration of 200 × 100 pixels produced relative changes of approximately 4.01–8.25%, while varying the Gaussian standard deviation from $\sigma = 2$ produced changes of approximately 3.28–9.89%; the tested Canny threshold settings, by contrast, produced substantially smaller changes, generally below 0.30%. These findings indicate that fractal-dimension estimates depend more strongly on spatial resolution and the degree of smoothing applied before edge extraction than on the edge-detection threshold itself.

3.4 K-NN Classification Results

Classification performance was evaluated using four-fold-count schemes: 3-fold, 5-fold, 7-fold, and 10-fold cross-validation, combined with four K values, resulting in 16 experimental combinations. Each combination was repeated using 10 random seeds.

Table 5. Repeated Stratified Cross-Validation Accuracy

Fold Scheme	K	Accuracy
3	3	85.14 ± 1.96
	5	84.36 ± 2.42
	7	82.64 ± 2.33
	9	81.71 ± 2.48
5	3	86.71 ± 0.84
	5	85.21 ± 1.54
	7	83.79 ± 1.39
	9	84.43 ± 1.16
7	3	86.64 ± 1.47
	5	84.71 ± 1.94
	7	83.29 ± 1.13
	9	84.36 ± 1.19
10	**3**	**87.14 ± 0.48**
	5	85.21 ± 1.35
	7	83.21 ± 0.97
	9	84.79 ± 0.96

To assess whether the observed advantage of K = 3 was statistically meaningful, paired Wilcoxon signed-rank tests were conducted using the ten seed-level accuracies from the 10-fold experiments. K = 3 significantly outperformed K = 5 (mean difference = 1.93 percentage points, Holm-adjusted p = 0.00391), K = 7 (3.93 percentage points, p = 0.00586), and K = 9 (2.35 percentage points, p = 0.00391). Thus, within the 10-fold evaluation, K = 3 showed a statistically significant advantage over the other tested neighborhood sizes after correction for multiple comparisons. This supports the designation of 10-fold with K = 3 as the best-performing observed configuration, while the conclusion remains specific to the evaluated dataset and experimental settings.

As shown in Table 5, the highest observed mean accuracy, 87.14% ± 0.48%, was obtained using the 10-fold scheme with K = 3, which was accordingly designated the best-performing observed configuration. Across all fold schemes, K = 3 consistently produced the highest mean accuracy among the tested K values, suggesting that with only 20 images per species, larger neighborhoods are more likely to include samples from adjacent classes and thereby reduce classification precision. The reported standard deviations in Table 5 were calculated across the ten seed-level accuracies for each configuration, providing a measure of variation across repeated random-seed evaluations.

The seed level standard deviation was generally larger for configurations with fewer folds, whereas the 10-fold, K = 3 configuration showed the smallest standard deviation (0.48%). The variability of cross-validation estimates is affected by fold selection and sample size; with a limited dataset, changes in the number of observations assigned to each validation subset can alter the influence of individual misclassifications on the resulting accuracy estimates [31].

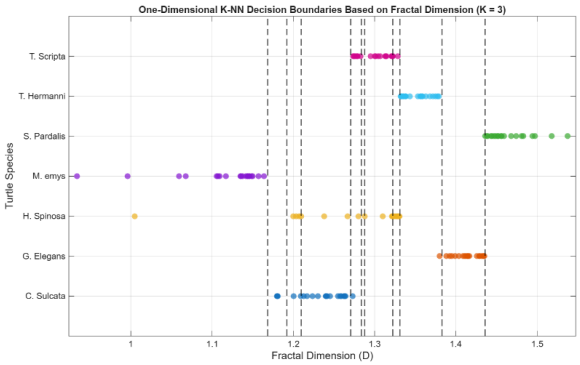


Figure 4. One-Dimensional K-NN Decision Boundaries Based on Fractal Dimension (K=3)

Figure 4 illustrates the one-dimensional K-NN decision boundaries obtained using fractal dimension as the sole input feature (K = 3). The distribution of fractal-dimension values shows that several species occupied relatively distinct regions along the fractal-dimension axis, particularly *Stigmochelys pardalis*, *Geochelone elegans*, and *Manouria emys*. However, substantial overlap was observed among species with similar fractal-dimension values, especially *Heosemys spinosa*, *Centrochelys sulcata*, and *Trachemys scripta elegans*. These overlapping regions indicate that a single fractal-dimension feature does not completely separate all species and are consistent with the misclassification patterns observed in the confusion matrix, particularly the misclassification of *H. spinosa* and *T. scripta*.

3.5 Class Wise Performance

For the best-performing observed configuration, namely 10-fold cross-validation with K = 3, the pooled confusion matrix across the 10 random seeds was evaluated using 1,400 validation predictions.

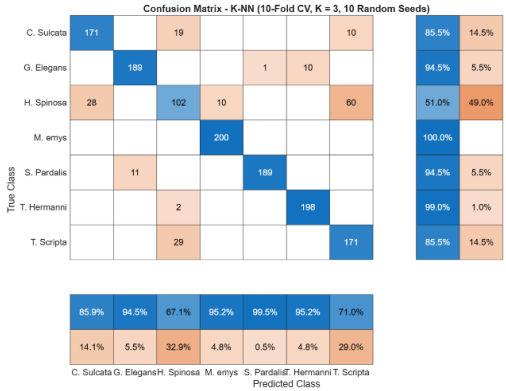


Figure 5. Confusion Matrix of the Best-Performing Observed Configuration

The confusion matrix shows a high number of correct predictions for several species, particularly Manouria emys, Stigmochelys pardalis, and Testudo hermanni, whereas Heosemys spinosa was more frequently confused with Centrochelys sulcata and Trachemys scripta elegans, reflecting overlap within the one-dimensional fractal-dimension feature space.

Table 6. Class Wise Performance for the Best-Performing Observed Configuration

Species	Precision	Recall	F1-Score
Trachemys scripta elegans	70.95%	85.50%	77.55%
Manouria emys	95.24%	100.00%	97.56%
Centrochelys sulcata	85.93%	85.50%	85.71%
Geochelone elegans	94.50%	94.50%	94.50%
Stigmochelys pardalis	99.47%	94.50%	96.92%
Testudo hermanni	95.19%	99.00%	97.06%
Heosemys spinosa	67.11%	51.00%	57.95%
Macro Average	**86.91%**	**87.14%**	**86.75%**

The class-wise results indicate relatively strong classification performance for *Manouria emys, Stigmochelys pardalis, Testudo hermanni, and Geochelone elegans.* In contrast, *Heosemys spinosa* showed the lowest recall (51.00%) and F1-score (57.95%), while *Trachemys scripta elegans* showed lower precision (70.95%) than the higher-performing species. These results indicate that a single fractal-dimension value can capture broad differences in carapace complexity but may be insufficient to distinguish species whose one-dimensional fractal-dimension distributions overlap.

The overlap between Heosemys spinosa and Trachemys scripta elegans is plausible on both biological and acquisition grounds. Biologically, although H. spinosa is nominally characterized by sharply serrated marginal scutes, this serration is most pronounced in juveniles and becomes visually subtler on adult carapaces, which can shift its edge-detected boundary complexity closer to the smoother-margined T. scripta elegans; the two species also share a broadly similar oval carapace outline, unlike the more visually distinctive star-shaped or heavily domed patterns of species such as Geochelone elegans or Stigmochelys pardalis. From an acquisition standpoint, citizen-science photographs of both species vary in viewing angle and distance, and because the sensitivity analysis (Section 2.3/3.3) shows that the extracted fractal dimension is sensitive to effective image resolution, any systematic similarity in how these two species happen to be commonly photographed on iNaturalist (for example, similar typical framing) could further narrow their separation in fractal-dimension space beyond what carapace pattern alone would produce. Distinguishing these two explanations would require a species-stratified image-quality audit, which is identified as future work in Section 3.7.

Compared with previous computational approaches to turtle species identification, which have predominantly relied on deep learning, the present study investigated a single numerical feature, box-counting fractal dimension, as a descriptor of carapace pattern complexity. Prior work has applied deep learning to turtle image classification, including the classification of turtles imported into Korea [9] and ensemble-based classification of turtle species [10]. A multiview ensemble combining YOLOv8 with a convolutional neural network has also been used for the automated, fine-grained classification of three closely related turtle species within the genus *Malayemys* [8].

In the present study, box-counting fractal dimension combined with K-NN achieved a best-performing observed accuracy of 87.14% ± 0.48% using a single numerical feature extracted from carapace patterns, indicating that fractal dimension carries information capable of supporting turtle species classification. Because the datasets, image conditions, species composition, and experimental protocols differ from those of previous deep-learning studies, those results cannot be directly compared with the present result; the comparison should instead be interpreted as an evaluation of the classification capability of fractal dimension within the present dataset. A controlled dataset matched comparison with GLCM features is therefore presented below.

3.6 Dataset Matched Baseline Comparison

To provide a controlled baseline comparison, GLCM features consisting of contrast, correlation, energy, and homogeneity were extracted from the same 140 images and classified using the same K-NN procedure, fold-count schemes, K values, and ten fixed random seeds. For reference, when GLCM was allowed to use its own best-performing configuration among the same 16-fold/K combinations (7-fold cross-validation with $K = 9$, distinct from fractal dimension's own-best setting of 10-fold, $K = 3$), it achieved 62.43% ± 2.43% accuracy and 61.78% macro-F1 essentially unchanged from its matched-setting result below, indicating that GLCM's ceiling performance was not substantially higher under its own optimal configuration. All formal statistical comparisons reported in this section, however, use the dataset-matched, identical 10-fold, $K = 3$ setting for both methods, so that any performance difference reflects the feature representation rather than a difference in cross-validation configuration. Under this matched 10-fold, $K = 3$ setting, fractal dimension achieved 87.14% ± 0.48% accuracy and 86.75% macro-F1, compared with 61.14% ± 1.76% and 60.17% for GLCM, respectively. The mean accuracy difference of 26.00 percentage points was statistically significant based on both the paired t-test ($t(9) = 43.01$, $p < 0.001$) and Wilcoxon signed-rank test ($p = 0.001953$), with a nominally very large paired effect (Cohen's $dz = 13.60$). These paired tests treat the ten random seeds as the unit of replication; because all ten seeds reuse the same 140 images and differ only in fold partitioning, they are not fully independent replicates, which inflates the apparent statistical power and the resulting effect-size magnitude relative to what would be obtained from ten independent samples. The paired tests and the exact Wilcoxon p-value are therefore best interpreted as a controlled, dataset-matched comparison confirming a consistent and practically large accuracy gap, rather than as an estimate of a generalizable effect size of magnitude 13.60 in the conventional sense.

It is also worth considering why fractal dimension outperformed the GLCM baseline by as much as 26 percentage points. One explanation is that fractal dimension is a genuinely more discriminative representation of carapace scute-boundary complexity than the selected GLCM descriptors. However, an alternative explanation is that the two feature pipelines were not preprocessed symmetrically: fractal dimension was computed from a carapace-cropped, Gaussian-smoothed, Otsu-segmented, and Canny-edge-detected image, whereas the original GLCM baseline was computed directly from the grayscale image without a comparable segmentation stage. To test this directly, an additional GLCM variant was computed using the same Otsu thresholding as the fractal-dimension branch, applied as a binary mask to isolate the carapace region while

preserving the original grayscale pixel values within that region for GLCM extraction (full Canny edge detection was not applied to the GLCM branch, since collapsing the image to a binary edge map would remove the gray-level variation GLCM requires, making the comparison meaningless rather than fairer). Under the matched 10-fold, K = 3 setting, this Otsu-masked GLCM variant achieved 55.07% ± 1.76% accuracy and 53.49% macro-F1 lower than, not higher than, the original unmasked GLCM baseline (61.14% ± 1.76%), and the gap relative to fractal dimension widened to 32.07 percentage points (paired t-test, $t(9) = 51.31$, $p = 2.04 \times 10^{-12}$; Wilcoxon signed-rank, $p = 0.001953$; Cohen's $d_z = 16.23$). This result indicates that the performance gap is not attributable to fractal dimension's additional preprocessing steps; if anything, region-masking degraded GLCM performance, plausibly because Otsu mask coverage varied substantially across images (mean 49.0%, SD 12.9%, range 11.3–97.0%), introducing a source of feature variability unrelated to species identity.

These findings indicate that the fractal-dimension representation provided greater discriminative information than the selected GLCM descriptors for the present dataset and parameter settings. However, the relatively small sample size (20 images per species) and reliance on a single fractal-dimension feature may limit generalizability and representation of other carapace characteristics. In addition, box-counting estimates can be sensitive to boundary complexity and scale range [16].

Table 7. Comparison of Fractal Dimension and GLCM-Based K-NN on the Same Dataset

Method or Configuration	Accuracy	Macro-F1	Mean Difference
Fractal dimension + K-NN (10-fold, K = 3)	87.14 ± 0.48%	86.75%	—
GLCM + K-NN (10-fold, K = 3)	61.14 ± 1.76%	60.17%	26.00 percentage points
GLCM + K-NN Otsu-masked + KNN (10-fold, K = 3)	55.07 ± 1.76%	53.49%	32.07 percentage points
GLCM + K-NN (best observed: 7-fold, K = 9)	62.43 ± 2.43%	61.78%	—

3.7 Limitations and Future Work

The present study has several limitations, and the performance figures reported above should be interpreted with these constraints in mind rather than as evidence of broad applicability. First, twenty images per species is a small sample for a seven-class problem and is the principal threat to generalizability; all performance claims in this study should accordingly be read as observations on this specific dataset rather than as general claims about turtle carapace classification. Relatedly, because the best-performing configuration (10-fold, K = 3) was selected post hoc from 16-fold/K combinations and then evaluated for statistical significance on the same data, the reported accuracy for this configuration is an optimistic, selection-biased estimate rather than an unbiased estimate of performance on unseen configurations. Second, the analysis used a single fractal-dimension feature, so species with overlapping one-dimensional distributions may remain difficult to distinguish. Third, the sensitivity analysis considered image resizing, Gaussian smoothing, and Canny thresholding, but did not independently vary crop tightness or Otsu thresholding. Fourth, citizen-science images sourced from iNaturalist vary in camera angle, lighting, and camera hardware; because the sensitivity analysis (Section 3.3) showed that fractal dimension is sensitive to image resolution and smoothing, uncontrolled heterogeneity in acquisition conditions is a genuine potential confound, since any systematic correlation between species and acquisition conditions (for example, if one species' observations were disproportionately photographed at closer range or under different lighting) could inflate apparent separability beyond what the carapace pattern itself would produce. A formal image-quality audit across species was not performed in this study and is recommended for future work. Finally, no independent external dataset was used for validation. Future research should evaluate larger and more diverse datasets, incorporate complementary shape, texture, or color features, compare a broader range of baseline representations, audit image-quality variation across species, and perform independent external validation. Because the images were randomly selected from publicly available iNaturalist Research Grade observations, repeating the selection process may produce a different image composition even when the same inclusion criteria are applied. Therefore, the reported results are reproducible with respect to the documented computational protocol rather than as an exact reconstruction of an identical image sample; the observation-ID deposit described below (Data and Code Availability) allows the exact sample used here to be reconstructed despite this protocol-level reproducibility limitation.

4. CONCLUSION

This study investigated box-counting fractal dimension as a numerical descriptor of turtle carapace pattern complexity and evaluated its use with K-NN classification across seven turtle species. Fractal dimension was found to capture meaningful differences in the extracted carapace patterns and to support species classification, with 10-fold stratified cross-validation at K = 3 yielding the best-performing observed accuracy of 87.14% ± 0.48% and a pooled macro-F1 of 86.75%. The class-wise analysis showed strong performance for several species, although substantial overlap remained for Heosemys spinosa and Trachemys scripta elegans, and the sensitivity analysis indicated that fractal-dimension values were affected more by image resizing and Gaussian smoothing than by the tested Canny threshold settings. On the same dataset and under the same 10-fold, K = 3 evaluation setting, the GLCM baseline achieved 61.14% ± 1.76% accuracy, with the paired comparison indicating a statistically significant difference between the two representations. Nevertheless, the limited dataset, single-feature representation, preprocessing dependence, and lack of external validation constrain the generalizability of the findings. Future research should therefore investigate larger datasets, complementary or fused image features, alternative baseline configurations, and independent validation. In the spirit of open science, the MATLAB code (image preprocessing, sensitivity analysis, fractal dimension calculation, GLCM extraction, and K-NN classification) and the complete list of 140 iNaturalist observation IDs and URLs used in this study have been deposited in a public repository.
(GitHub, with a permanent archived snapshot via Zenodo: https://github.com/nadyanafis/Turtle-Fractal-Dimension-KNN) under DOI https://doi.org/10.5281/zenodo.22725148, to directly support both code reproducibility and sample level reproducibility of the reported results [32].

5. REFERENCES

[1] C. Chen, J. Wang, M. Holyoak, L. Lin, and Y. Wang, "Global assessment of current extinction risks and future challenges for turtles and tortoises," *Nature Communications 2025 16:1*, vol. 16, no. 1, pp. 7114-, Aug. 2025, doi: 10.1038/s41467-025-62441-2.

[2] N. Cox *et al.*, "A global reptile assessment highlights shared conservation needs of tetrapods," *Nature 2022 605:7909*, vol. 605, no. 7909, pp. 285–290, Apr. 2022, doi: 10.1038/s41586-022-04664-7.

[3] V. Nijman and C. R. Shepherd, "Trade in Southeast Asian Box Turtles from Indonesia: Legality, Livelihoods, Sustainability and Overexploitation," *Diversity 2022, Vol. 14, Page 970*, vol. 14, no. 11, p. 970, Nov. 2022, doi: 10.3390/D14110970.

[4] V. Nijman and C. R. Shepherd, "Legal freshwater turtle meat trade in Indonesia only marginally contributes to collectors' livelihoods," *Discover Animals 2025 2:1*, vol. 2, no. 1, pp. 17-, Mar. 2025, doi: 10.1007/S44338-025-00062-1.

[5] C. Y. Hau, W. K. Ngan, and Y. Sadovy de Mitcheson, "Leveraging artificial intelligence for photo identification to aid CITES enforcement in combating illegal trade of the endangered humphead wrasse (Cheilinus undulatus)," *Front. Ecol. Evol.*, vol. 13, p. 1526661, Mar. 2025, doi: 10.3389/FEVO.2025.1526661/TEXT.

[6] S. Su, D. Gu, J. Y. Lai, N. Arcilla, and T. Y. Su, "A novel deep learning-based bioacoustic approach for identification of look-alike white-eye (Zosterops) species traded in wildlife markets," *Ibis*, vol. 167, no. 1, pp. 41–55, Jan. 2025, doi: 10.1111/IBI.13309;REQUESTEDJOURNAL:JOURNAL:1474919X;WGROUP:STRING:PUBLICATION.

[7] E. Eravci Yalin *et al.*, "Carapace Morphology Variations in Captive Tortoises: Insights from Three-Dimensional Analysis," *Animals 2024, Vol. 14, Page 2664*, vol. 14, no. 18, p. 2664, Sep. 2024, doi: 10.3390/ANI14182664.

[8] W. Songpan, T. Chaianunporn, K. Lomthaisong, and S. Keithmaleesatti, "Automated classification in turtles genus Malayemys using ensemble multiview image based on improved YOLOv8 with CNN," *Scientific Reports 2024 14:1*, vol. 14, no. 1, pp. 24993-, Oct. 2024, doi: 10.1038/s41598-024-76431-9.

[9] J. W. Baek, J. Il Kim, and C. B. Kim, "Deep learning-based image classification of turtles imported into Korea," *Scientific Reports 2023 13:1*, vol. 13, no. 1, pp. 21677-, Dec. 2023, doi: 10.1038/s41598-023-49022-3.

[10] R. Faurina, A. Wijanarko, A. F. Heryuanti, S. I. Ishak, and I. Agustian, "Comparative study of ensemble deep learning models to determine the classification of turtle species," *Computer Science and Information Technologies*, vol. 4, no. 1, pp. 24–32, Mar. 2023, doi: 10.11591/CSIT.V4I1.P24-32.

[11] S. Binta Islam, D. Valles, T. J. Hibbitts, W. A. Ryberg, D. K. Walkup, and M. R. J. Forstner, "Animal Species Recognition with Deep Convolutional Neural Networks from Ecological Camera Trap Images," *Animals 2023, Vol. 13, Page 1526*, vol. 13, no. 9, p. 1526, May 2023, doi: 10.3390/ANI13091526.

[12] K. Seljebotn and I. A. Lawal, "Machine Learning Tool for Wildlife Image Classification," *ACM International Conference Proceeding Series*, pp. 127–132, May 2024, doi: 10.1145/3674029.3674050;CSUBTYPE:STRING:CONFERENCE.

[13] K. Tabuki, H. Nishizawa, O. Abe, J. Okuyama, and S. Tanizaki, "Utility of carapace images for long-term photographic identification of nesting green turtles," *J. Exp. Mar. Biol. Ecol.*, vol. 545, p. 151632, Dec. 2021, doi: 10.1016/J.JEMBE.2021.151632.

[14] R. W. Burroughs, J. F. Parham, B. L. Stuart, P. D. Smits, and K. D. Angielczyk, "Morphological Species Delimitation in The Western Pond Turtle (Actinemys): Can Machine Learning Methods Aid in Cryptic Species Identification?," *Integrative Organismal Biology*, vol. 6, no. 1, Jan. 2024, doi: 10.1093/IOB/OBAE010.

[15] W. Jiang, Y. Liu, J. Wang, R. Li, X. Liu, and J. Zhang, "Problems of the Grid Size Selection in Differential Box-Counting (DBC) Methods and an Improvement Strategy," *Entropy 2022, Vol. 24, Page 977*, vol. 24, no. 7, p. 977, Jul. 2022, doi: 10.3390/E24070977.

[16] V. Muraleedharan, S. C. Rajan, and J. R, "Determining the limits of traditional box-counting fractal analysis in leaf complexity studies," *Flora*, vol. 304, p. 152300, Jul. 2023, doi: 10.1016/J.FLORA.2023.152300.

[17] G. Taraschi and J. B. Florindo, "Computing fractal descriptors of texture images using sliding boxes: An application to the identification of Brazilian plant species," *Physica A: Statistical Mechanics and its Applications*, vol. 545, p. 123651, May 2020, doi: 10.1016/J.PHYSA.2019.123651.

[18] C. Khotimah and D. Juniati, "Iris Recognition Using Feature Extraction of Box Counting Fractal Dimension," *J. Phys. Conf. Ser.*, vol. 947, no. 1, p. 012004, Jan. 2018, doi: 10.1088/1742-6596/947/1/012004.

[19] K. Mahapatra, S. R, K. Mahapatra, and S. R, "Fractal Dimension and Entropy Analysis of Medical Images for KNN-Based Disease Classification," *Baghdad Science Journal*, vol. 22, no. 4, pp. 1354–1365, Apr. 2025, doi: 10.21123/bsj.2024.10835.

[20] R. Padhy, S. K. Dash, A. Khandual, and J. Mishra, "Image classification in artificial neural network using fractal dimension," *International Journal of Information Technology 2023 15:6*, vol. 15, no. 6, pp. 3003–3013, Jun. 2023, doi: 10.1007/S41870-023-01318-3.

[21] P. Langley *et al.*, "Fractal dimension to classify the heart sound recordings with KNN and fuzzy c-mean clustering methods," *J. Phys. Conf. Ser.*, vol. 953, no. 1, p. 012202, Jan. 2018, doi: 10.1088/1742-6596/953/1/012202.

[22] N. Iqbal, R. Mumtaz, U. Shafi, and S. M. H. Zaidi, "Gray level co-occurrence matrix (GLCM) texture based crop classification using low altitude remote sensing platforms," *PeerJ Comput. Sci.*, vol. 7, pp. 1–26, May 2021, doi: 10.7717/PEERJ-CS.536/TABLE-21.

[23] Kiswanto, H. Hadiyanto, and E. Sediyono, "Evaluation of Wavelet and Gray Level Co-Occurrence Matrix Combination Model for Texture Image Feature Extraction of Various Types of Meat," *Ingenierie des Systemes d'Information*, vol. 30, no. 4, pp. 933–943, Apr. 2025, doi: 10.18280/ISI.300410.

[24] T. M. Cover and P. E. Hart, "Nearest Neighbor Pattern Classification," *IEEE Trans. Inf. Theory*, vol. 13, no. 1, pp. 21–27, 1967, doi: 10.1109/TIT.1967.1053964.

[25] "Centrochelys sulcata: Petrozzi, F., Luiselli, L., Hema, E.M., Diagne, T., Segniagbeto, G.H., Eniang, E.A., Leuteritz, T.E.J. & Rhodin, A.G.J.," *IUCN Red List of Threatened Species*, Aug. 2020, doi: 10.2305/IUCN.UK.2021-1.RLTS.T163423A1006958.EN.

[26] "Checklist - Tortoise and Freshwater Turtle Specialist Group." Accessed: Aug. 27, 2026. [Online]. Available: https://iucn-tftsg.org/checklists/

[27] N. Otsu, "THRESHOLD SELECTION METHOD FROM GRAY-LEVEL HISTOGRAMS.," *IEEE Trans Syst Man Cybern*, vol. SMC-9, no. 1, pp. 62–66, 1979, doi: 10.1109/TSMC.1979.4310076.

[28] J. Canny, "A Computational Approach to Edge Detection," *IEEE Trans. Pattern Anal. Mach. Intell.*, vol. PAMI-8, no. 6, pp. 679–698, 1986, doi: 10.1109/TPAMI.1986.4767851.

[29] D. Juniati and I. K. Budayasa, *Geometri Fraktal dan Aplikasinya*. Surabaya: Unesa University Press, 2016.

[30] S. Prusty, S. Patnaik, and S. K. Dash, "SKCV: Stratified K-fold cross-validation on ML classifiers for predicting cervical cancer," *Frontiers in Nanotechnology*, vol. 4, p. 972421, Aug. 2022, doi: 10.3389/FNANO.2022.972421/TEXT.

[31] T. Abedin, H. Xu, and S. Uddin, "The impact of K selection in K-fold cross-validation on bias and variance in supervised learning models," *Scientific Reports 2026 16:1*, vol. 16, no. 1, pp. 6084-, Jan. 2026, doi: 10.1038/s41598-026-37247-x.

[32] Nadyanafis, nadyanafis/Turtle-Fractal-Dimension-KNN: Initial release for journal submission. (Sep. 12, 2026). Zenodo. doi: 10.5281/zenodo.22725148.